frontiers in Physics

BRIEF RESEARCH REPORT
published: 24 December 2021
doi: 10.3389/fphy.2021.785801

The Transport Properties of Quasi–One-Dimensional $Ba_3Co_2O_6(CO_3)_{0.7}$

*Minnan Chen[1], Jiangtao Wu[1], Qing Huang[2], Jinlong Jiao[1], Zhiling Dun[3], Guohua Wang[1], Zhiwei Chen[4], Gaoting Lin[1], Vasudevan Rathinam[1], Cangjin Li[5], Yanzhong Pei[5], Feng Ye[6], Haidong Zhou[2] and Jie Ma[1,7]**

[1]Key Laboratory of Artificial Structures and Quantum Control, School of Physics and Astronomy, Shanghai Jiao Tong University, Shanghai, China, [2]Department of Physics and Astronomy, University of Tennessee, Knoxville, TN, United States, [3]School of Physics, Georgia Institute of Technology, Atlanta, GA, United States, [4]Center for Phononics and Thermal Energy Science, Shanghai Key Laboratory of Special Artificial Microstructure Materials and Technology, School of Physics Science and Engineering, Tongji University, Shanghai, China, [5]Interdisciplinary Materials Research Center, School of Materials Science and Engineering, Tongji University, Shanghai, China, [6]Neutron Scattering Division, Oak Ridge National Laboratory, Oak Ridge, TN, United States, [7]Wuhan National High Magnetic Field Center, Huazhong University of Science and Technology, Wuhan, China*

We have performed combined elastic neutron diffuse, electrical transport, specific heat, and thermal conductivity measurements on the quasi–one-dimensional $Ba_3Co_2O_6(CO_3)_{0.7}$ single crystal to characterize its transport properties. A modulated superstructure of polyatomic CO_3^{2-} is formed, which not only interferes the electronic properties of this compound, but also reduces the thermal conductivity along the c-axis. Furthermore, a large magnetic entropy is observed to be contributed to the heat conduction. Our investigations reveal the influence of both structural and magnetic effects on its transport properties and suggest a theoretical improvement on the thermoelectric materials by building up superlattice with conducting ionic group.

Keywords: cobalt oxide, neutron diffuse, spin entropy, carrier mobility, thermal conductivity, scattering mechanism

OPEN ACCESS

Edited by:
Gang Zhang,
*Technology and Research (A*STAR), Singapore*

Reviewed by:
Ke-Qiu Chen,
Hunan University, China
Zhi Zeng,
Hefei Institutes of Physical Science (CAS), China

****Correspondence:***
Jie Ma
jma3@sjtu.edu.cn

Specialty section:
This article was submitted to Condensed Matter Physics, a section of the journal Frontiers in Physics

Received: *29 September 2021*
Accepted: *19 November 2021*
Published: *24 December 2021*

Citation:
Chen M, Wu J, Huang Q, Jiao J, Dun Z, Wang G, Chen Z, Lin G, Rathinam V, Li C, Pei Y, Ye F, Zhou H and Ma J (2021) The Transport Properties of Quasi–One-Dimensional $Ba_3Co_2O_6(CO_3)_{0.7}$. Front. Phys. 9:785801. doi: 10.3389/fphy.2021.785801

INTRODUCTION

Thermoelectric (TE) materials can recycle waste heat into usable electricity based on the Seebeck effect and are believed to play a significant role in efficient use of energy [1]. As the energy conversion performance of TE materials is evaluated by the dimensionless figure of merit zT, $zT = S^2\sigma T/(\kappa_{ele} + \kappa_{latt})$, where T is operating temperature, σ is electrical conductivity, S is Seebeck coefficient, κ_{ele} is electronic thermal conductivity, and κ_{latt} is lattice thermal conductivity, the research on the TE material is usually focused on two main approaches: (1) increasing the power factor $S^2\sigma$ through electronic structure or energy band engineering [2–4] and (2) reducing the lattice thermal conductivity κ_{latt} by introducing additional phonon scattering and manipulating phonon structure [5–9]. Actually, those approaches are very complex. For example, the electrical transport ($\sigma = n\mu e$) could be regulated by the carrier concentration n, the carrier mobility μ, and the electron charge e, whereas the acoustic phonon scattering introduces a $\mu \propto T^{-1.5}$ dependence, and the ionized impurity scattering gives a $\mu \propto T^{1.5}$ relationship [10]. Furthermore, the lattice thermal conductivity, κ_{latt}, could be decreased by the grain boundary scattering, point defect scattering, disorder scattering, and Umklapp scattering [11, 12]. Therefore, if the scattering mechanisms of both the electrical and thermal transport could be well understood, the energy conversion performance of TE materials can be better optimized.

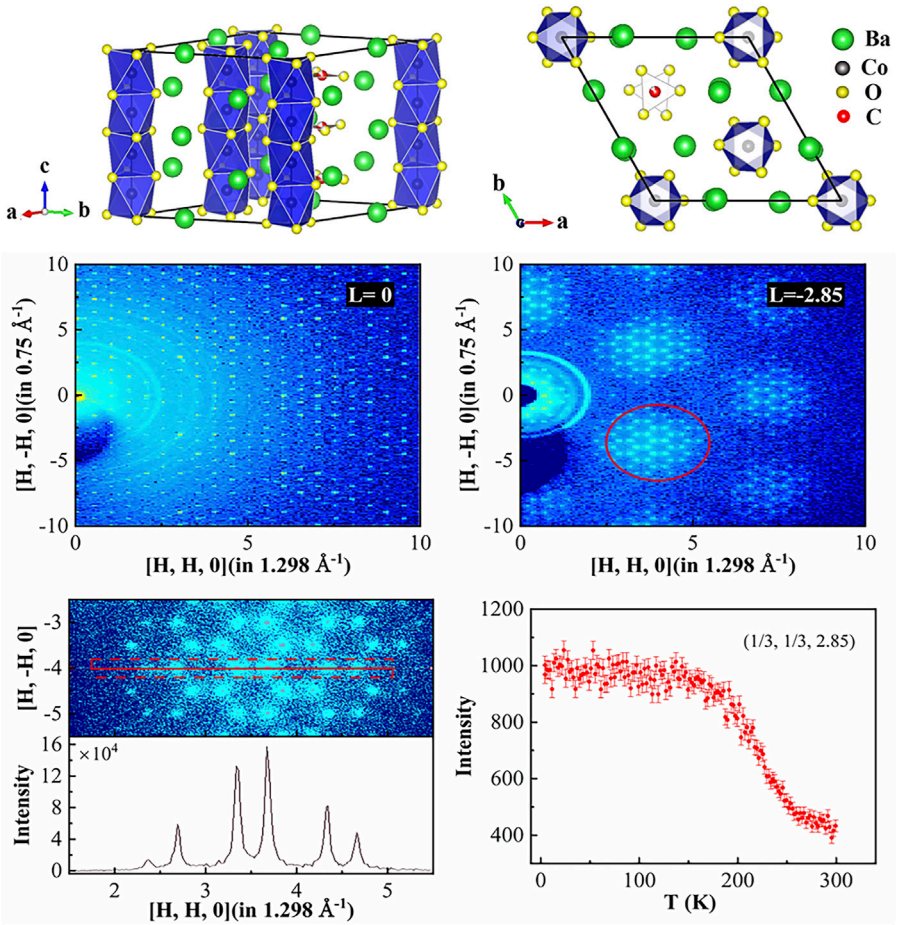

FIGURE 1 | (A) Crystal structure of $Ba_3Co_2O_6(CO_3)_{0.7}$ consisting of chains of CoO_6 and carbonate CO_3 along the c-axis in the standard orientation [space group: P-6]. **(B)** The c-axis projected crystal structure. 2D slice of diffuse neutron scattering patterns of $Ba_3Co_2O_6(CO_3)_{0.7}$ single crystal at 50 K. **(C)** $L = 0$, **(D)** $L = -2.85$, and **(E)** enlarged view of a section of **(D)** obtained on CORELLI. **(F)** Cuts along the [H, H, 0] direction of the Bragg peak marked by red solid line in panel **(E)**. **(G)** Temperature dependence of the peak intensity of the (1/3 1/3 2.85).

At present, alloy TE materials have been widely applied as a TE compound. Although the performance has been continuously improved, there are some unavoidable limitations on the environment, expenses, oxidization stability, and so on [13–15]. Therefore, the investigation of oxide TE materials has been proposed. Because of its special crystal structure and magnetic effect, the cobalt oxide has good electronic properties and low lattice thermal conductivity [16–21]. For example, the power factor ($S^2\sigma$) of $NaCo_2O_4$ is 5×10^{-3} W · m^{-1} · K^{-2}, even higher than that of Bi_2Te_3 [22]. Among them, $NaCo_2O_4$, $Ca_3Co_4O_9$, and $Bi_2Sr_2Co_2O_x$ have received much attention, and their TE performance is also continuously improved and even higher than some alloys [17, 23–26].

Recently, a quasi–one-dimensional cobaltate $Ba_3Co_2O_6(CO_3)_{0.7}$ has been reported as a new excellent potential TE material [27]. This compound comprised face-sharing CoO_6 octahedra and carbonate CO_3^{2-} molecular chains along its c-axis with the space group of P-6, $a = 9.683$ Å and $c = 9.518$ Å [28], **Figures 1A, B**. The average occupancy of the polyatomic CO_3^{2-} molecule is 0.7. Although z of $Ba_3Co_2O_6(CO_3)_{0.7}$ was reported as 5.1×10^{-5} K^{-1}, which is comparable to NaxCoO$_2$-y at 300 K, and it was considered as a promising cobalt oxide TE material [24], the thermal conductivity, transport properties, and the physics remain unknown.

In this article, we report neutron diffuse scattering, electrical conductivity, Hall effect, specific heat, and thermal conductivity of $Ba_3Co_2O_6(CO_3)_{0.7}$ single crystal. Moreover, the magnetic effect of the Co ions is discussed.

EXPERIMENTAL DETAILS

Single crystal of $Ba_3Co_2O_6(CO_3)_{0.7}$ was grown by a flux method using a mixture of Co_3O_4, $BaCO_3$, K_2CO_3, and $BaCl_2$ [27]. These single crystals have the shape of short hexagonal rods. The c-axis was determined using the X-ray Laue method to be along the rod direction.

A single crystal with dimension of $2 \times 2 \times 6$ mm^3 was aligned in the (H, K, 0) horizontal scattering plane for the diffuse

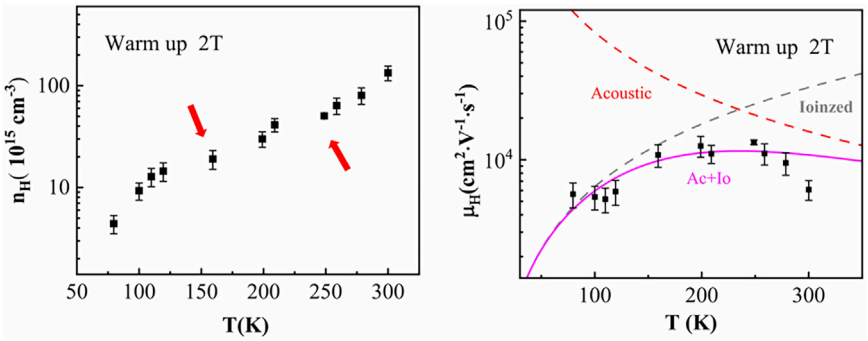

FIGURE 2 | Temperature dependence of **(A)** carrier concentration n_H and **(B)** Hall mobility μ_H along the c-axis for $Ba_3Co_2O_6(CO_3)_{0.7}$. **(B)** Calculated carrier mobility (magenta solid line) took into account the ionized impurity scattering (gray dashed line) and acoustic phonon scattering (red dashed line) contributions.

scattering studies using the elastic single crystal diffuse scattering spectrometer CORELLI at the Spallation Neutron Source (SNS), Oak Ridge Nation Laboratory [29]. Based on the Hall effect, the carrier concentration of $Ba_3Co_2O_6(CO_3)_{0.7}$ in the temperature range of 80 to 300 K was measured by the van der Pauw technique at a reversible magnetic field of 2 T. And the conductivity along the c-direction was obtained by Physical Property Measurement System (PPMS, Quantum Design) with resistivity option, using the four-probe method. The specific heat measurement was applied on PPMS's heat capacity option in two steps. First, the background specific heat was measured by an empty puck with a small amount of N-grease in the temperature range from 2 to 250 K at zero field. Then, a $Ba_3Co_2O_6$ $(CO_3)_{0.7}$ sample (approximately 4.71 mg) was placed in the measured N-grease, and the total specific heat was measured at same conditions. Finally, we gained the specific heat of the sample by subtracting the background specific heat from the total specific heat. The thermal conductivity along the c-axis was characterized using PPMS with thermal transport options, and the four-probe lead configuration method was used. During the measurement, the matching gold-plated copper bar in PPMS was used as leads. More detail for the measurement of carrier concentration, specific heat and thermal conductivity can be find in **Supplementary Material**. The diffuse scattering studies, carrier concentration, electrical conductivity, and thermal conductivity, were carried out on the same crystal, and the sample for the measurement of the specific heat was cut from this crystal too.

RESULTS AND DISCUSSION

Elastic Diffuse Scattering

To further understand the structural details of $Ba_3Co_2O_6(CO_3)_{0.7}$, we study the elastic diffuse scattering behavior of it. **Figures 1C, D** show the contour plot of neutron intensity at 50 K in the (H, K, 0) plane of $Ba_3Co_2O_6(CO_3)_{0.7}$ with $L = 0$ and $L = -2.85$. The sharp spots in **Figure 1C** demonstrate the good crystallinity of the single crystal. The signals of strong diffuse scattering are clearly observed at $L = -2.85$. **Figure 1F**, corresponding to the red solid line in **Figure 1E**, shows the elastic intensity along the [H, H, 0] direction and the relative diffuse intensity of each diffuse spot. Morgan et al. [30] have analyzed the short-range diffuse scattering using reverse Monte Carlo method and concluded that the diffuse scattering has short-range correlation between the disorder vibrations of polyatomic CO_3^{2-}.

Figure 1G shows the temperature dependence of the superlattice (1/3, 1/3, 2.85) reflection. Upon warming, the intensity starts to decrease at 150 K and approaches a T-independent constant greater than 250 K. Thus, the vibrations of polyatomic CO_3^{2-} should be affected by the thermal effect, and the localization of the CO_3^{2-} cluster should be relaxed.

Electrical Transport Properties

To obtain the electrical transport properties of $Ba_3Co_2O_6(CO_3)_{0.7}$ single crystal, Hall carrier concentration n_H was collected at a reversible magnetic field of 2 T, and Hall mobility μ_H was determined with zero-field resistivity, as shown in **Figure 2**. The exponential increase of carrier concentration with rising temperature indicates the thermal excitation of carriers. The charge polarity is dominated by holes in the measured temperature range, which is consistent with the positive Seebeck coefficients reported by Igarashi et al. [31]. The low carrier concentrations suggest that the further acceptor doping is required for TE applications. As marked in **Figure 2A**, there are two anomalies at 150 and 250 K, which agrees very well with the diffuse data and confirmed that CO_3^{2-} ion is a conductor in the system.

The temperature versus μ_H of $Ba_3Co_2O_6(CO_3)_{0.7}$ single crystal is nonmonotonic, as shown in **Figure 2B**. The calculated mobility involving both the ionized impurity scattering and acoustic phonon scattering can well match the experimental values over a wide temperature range. μ_H follows a temperature dependence closing to $T^{1.5}$ at low temperature range, implying that ionized impurity scattering dominates at low temperature in $Ba_3Co_2O_6(CO_3)_{0.7}$ single crystal. We believe that the ionized impurity scattering relates to polyatomic CO_3^{2-}. As the temperature increases, the localized ordering of CO_3^{2-} weakens, and the scattering of ionized impurity also diminishes. On the other hand, the lattice vibrations become

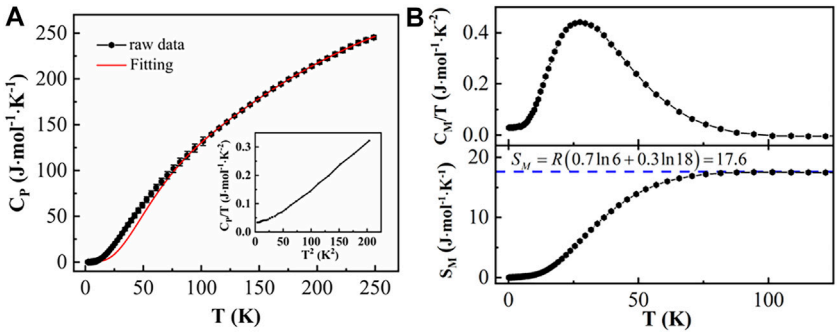

FIGURE 3 | (A) The total specific heat C_P of $Ba_3Co_2O_6(CO_3)_{0.7}$ measured at zero field. The red line represents the lattice contribution by **Eq. 1**. The inset shows the C_P/T vs T^2 **(B)** The magnetic specific heat is obtained by subtracting the lattice contribution C_p from the raw data. **(C)** Magnetic entropy obtained by integrating C_M/T over the entire measured temperature range.

stronger with increasing temperature. These two factors together lead to the acoustic phonon scattering, gradually overshadowing the ionized impurity scattering and becoming the dominant scattering mechanism in the material, which causes a negative temperature-dependence slope of μ_H greater than 250 K. The CO_3^{2-} is delocalized when $T > 250$ K, which might introduce other scattering mechanisms affecting the carriers transports and make the carrier mobility lower than the theoretical value.

Results of $C_P(T)$

To investigate the thermal effect in $Ba_3Co_2O_6(CO_3)_{0.7}$, the specific heat C_P was measured in the temperature range from 2 to 250 K at zero field. As shown in **Figure 3A**, the profile of data is very smooth, and no obvious peak is detected, indicating the absence of structure and magnetic transitions. The inset of **Figure 3A** displays the data as a C_P/T versus T^2. According to the Debye model, the lattice term of the total specific heat C_P/T is linear with T^2 at low T, but the data demonstrate a deviation from the linear relationship at low temperature and a nonzero intercept (approximately 0.29 J · mol^{-1} · K^{-2}) at 0 K. The nonzero intercept is an order of magnitude larger than that for $NaCo_2O_4$, which is a strongly correlated electronic cobalt system [32], and suggests $Ba_3Co_2O_6(CO_3)_{0.7}$ as also a strongly correlated electronic system.

In order to further study the specific heat of $Ba_3Co_2O_6(CO_3)_{0.7}$, a fitting was gained by using the Debye–Einstein model, which can fit the lattice specific heat data well at both low and high temperature. The model is written as follows [33]:

$$C_p(T) = C_D\left[9R\left(\frac{T}{\theta_D}\right)^3\int_0^{x_D}\frac{x^4e^x}{(e^x-1)^2}dx\right] + \sum_i C_{E_i}\left[3R\left(\frac{\theta_{E_i}}{T}\right)^2\frac{\exp\left(\frac{\theta_{E_i}}{T}\right)}{\left[\exp\left(\frac{\theta_{E_i}}{T}\right)-1\right]^2}\right], \quad (1)$$

where the first term is the contribution from the acoustic branch (Debye term), and the remaining terms are related to the contribution of the optical branch (Einstein terms). C_D and C_{Ei} are the relative weights of the Debye and Einstein terms,

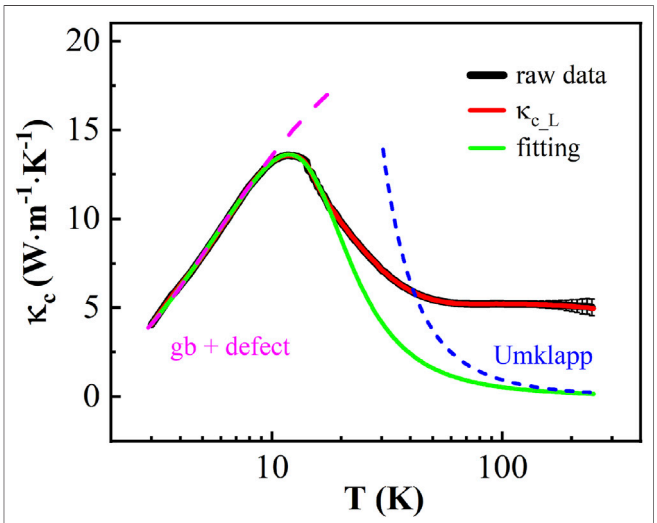

FIGURE 4 | The temperature dependence of the thermal conductivity κ_c and the lattice thermal conductivity (κ_{c_L}) along the c-axis of $Ba_3Co_2O_6(CO_3)_{0.7}$ at zero field. The black line is experimental data of the thermal conductivity; the red line is κ_{c_L}, and the green one represents the result of fitting by **Eq. 2**. The magenta dashed line is the contribution of the grain boundary and the point defect scattering, and the blue one is Umklapp process scattering.

respectively. R is the universal gas constant. θ_D and θ_{Ei} represent Debye and Einstein temperatures. There are 13.8 atoms per formula in our system. The best fitting for our data results is one Debye term and three E terms with a ratio 1:6:2.8:4 for C_D: C_{E1}:C_{E2}:C_{E3} and $\theta_D = 163$ K, $\theta_{E1} = 816$ K, $\theta_{E2} = 179$ K, and $\theta_{E3} = 290$ K, respectively.

As there is no distinct phase transition in the specific heat data, and the magnetic long-range order was not observed down to 2 K [34], the deviation of the experimental data from the fitted values indicates the presence of short-range magnetic fluctuations. **Figures 3B, C** display the magnetic specific heat, C_M, by subtracting the fitted lattice contribution from raw data, and the related magnetic entropy S_M, respectively. The S_M enhances with increasing temperature, and almost 100% recovered the theoretical value 17.6 J · mol^{-1} · K^{-1} at

approximately 100 K. Both contributions of spin and orbital degrees of freedom are suggested to be considered [35]: Co^{4+} has high-spin state with $S = 1/2$ ($3d^5$), and Co^{3+} has intermediate-spin state with $S = 1$ ($3d^6$), leading to $S_M = R(0.7 \ln 6 + 0.3 \ln 18) = 17.6\ J \cdot mol^{-1} \cdot K^{-1}$, as shown by the blue dotted line in **Figure 3C**. There may be spin-phonon scattering in the huge magnetic entropy regimen that interferes with the thermal conductivity.

Thermal Transport Properties

Figure 4 shows the temperature dependence of the total thermal conductivity κ_c and the lattice thermal conductivity κ_{c_L} of $Ba_3Co_2O_6(CO_3)_{0.7}$ parallel to the c-axis from 3 to 250 K κ_c consists of κ_{c_L} and the electronic thermal conductivity κ_{c_e}, where the electronic thermal conductivity can be determined by the Wiedemann–Franz law ($\kappa_e = \sigma L_n T$, where the Lorenz number $L_n = 2.45 \times 10^{-8}\ W \cdot \Omega \cdot K^{-2}$) and subtracted. At low temperatures, κ_c and κ_{c_L} almost completely overlap due to the very small electronic thermal conductivity. As the temperature increases, κ_c and κ_{c_L} begin to separate because of the exponential increase in conductivity. Although κ_{c_e} is maximum at 250 K, it is only a few percent of κ_{c_L}. The contribution of phonon to κ_c is domain. κ_{c_L} increases rapidly at low temperature with the dominant boundary scattering, which displays a $\kappa_{c\_L} \propto T^3$ dependence. A maximum with a value of $13.5\ W \cdot m^{-1} \cdot K^{-1}$ appears at approximately 12 K, where the Umklapp processes with exp (θ_D/bT) dependence become frequent and enough to compare with boundary scattering. One notes that the peak of κ_{c_L} is an order of magnitude smaller than that of other cobalt oxides, such as $Ca_3Co_2O_6$ [36]. This difference may be caused by the superlattice in $Ba_3Co_2O_6(CO_3)_{0.7}$, which can enhance the scatting of κ_{c_L}. As temperature increases further, κ_{c_L} drops very quickly and reflects that the Umklapp process scattering gradually becomes the main scattering mechanism. When the temperature is higher than 60 K, the trend of the curve gets flat. At approximately 250 K, the lattice thermal conductivity of $Ba_3Co_2O_6(CO_3)_{0.7}$ along the c-axis is $5.02\ W \cdot m^{-1} \cdot K^{-1}$.

The data of κ_{c_L} were fitted to the formula given by the Debye model of phonon thermal conductivity[37].

$$\kappa_{c\_L} = \frac{k_B}{2\pi^2 \nu_p}\left(\frac{k_B}{\hbar}\right)^3 T^3 \int_0^{\theta_D/T} \frac{x^4 e^x}{(e^x - 1)^2}\tau(\omega, T)dx, \quad (2)$$

where k_B is the Boltzmann's constant, ν_p is the average sound velocity, $\hbar$ is the Planck constant, $x = \hbar\omega/k_B T$, ω is frequency, and τ is the mean lifetime of phonon. The phonon relaxation is usually defined as follows:

$$\tau^{-1} = \nu_p/L + A\omega^4 + BT\omega^3 \exp(-\theta_D/bT). \quad (3)$$

These three items correspond with phonon boundary scattering, phonon point defect scattering, and the phonon–phonon Umklapp processes, respectively. L, A, B, and b are the fitting parameters. ν_p can be calculated by the Debye temperature $\theta_D = 163$ K obtained by the fitting above and **Eq. 4**:

$$\theta_D = \frac{\hbar\nu_p}{k_B}\left(\frac{6\pi^2 N}{V}\right)^{\frac{1}{3}} \quad (4)$$

where N is the number of atoms in crystal, and V is the volume of crystal, and then we obtain the average sound velocity of the sample $\nu_p \approx 1{,}343\ m \cdot s^{-1}$.

The best fitting is shown in **Figure 4** as green solid line with $L = 1.6 \times 10^{-5}$ m, $A = 1.7 \times 10^{-41}\ s^3$, $B = 7.4 \times 10^{-29}\ K^{-1}\ s^2$, and $b = 2.7$. The lattice thermal conductivity is mainly the contribution of phonons below approximately 18 K. As the temperature increases, the fitted values gradually deviate from the raw data. An extra contribution of the thermal conductivity has also been observed in $Ca_3Co_2O_6$ [38]. In combination with the heat capacity, the deviation of thermal conductivity might be due to the overestimation of the lattice thermal conductivity, because of the magnetic contribution to the total thermal conductivity: (1) The magnetic entropy increases rapidly after 18 K; in the meantime, κ_{c_L} starts to be higher than the theoretical value. (2) After the magnetic entropy reaches saturation at approximately 100 K, the κ_{c_L} also decreases slowly with growing temperature at the same rate as the theoretical one. As the electron concentration is very low, the electron–phonon scattering is not dominant in the system, and the CO_3^{2-} affects grain boundary and defect.

CONCLUSION

In summary, we have studied the structural, electrical, and thermal transport properties of quasi–one-dimensional $Ba_3Co_2O_6(CO_3)_{0.7}$ single crystal and the connection between the lattice structure, magnetism, and its transport properties. Neutron diffuse reveals that a modulated superstructure of CO_3^{2-} is formed in $Ba_3Co_2O_6(CO_3)_{0.7}$. The main hole carriers in the systems are continuously excited with increasing temperature and scattered not only by short-range ordered polyatomic CO_3^{2-} at low temperature, but also by acoustic phonon and nonlocalized CO_3^{2-} at high temperature. No lattice and magnetic phase transition are observed by the specific heat measurement, and the magnetic entropy is consistent with mixed Co^{3+} and Co^{4+} valence. The thermal conductivity of $Ba_3Co_2O_6(CO_3)_{0.7}$ shows an enhancement at higher temperatures over classic phonon heat transfer due to the contribution of the itinerant magnetism. The unique lattice and transport properties in $Ba_3Co_2O_6(CO_3)_{0.7}$ suggest a potential superlattice designs for regulating the TE properties.

DATA AVAILABILITY STATEMENT

The original contributions presented in the study are included in the article/**Supplementary Material**, further inquiries can be directed to the corresponding author.

AUTHOR CONTRIBUTIONS

MC and JM conceived the project. QH and HZ provided single crystals used in this study. FY and ZD performed neutron scattering experiments and analyzed the data with the help

from JM JW and VR. ZC, CL and YP performed carrier concentration measurement. MC performed specific heat and conductivity measurements and analyzed the data with the help with GW, GL and JJ. GW carried out the thermal property measurements. All authors discussed the results and contributed to the writing of the manuscript.

FUNDING

MC, JW, JJ, GW, GL, and JM thank the financial support from the National Science Foundation of China (Nos. 11774223, and U2032213), the interdisciplinary program Wuhan National High Magnetic Field Center (Grant No. WHMFC 202122), Huazhong University of Science and Technology, and the National Key Research and Development Program of China (Grant Nos. 2016YFA0300501 and 2018YFA0704300). GL thanks the project funded by China Postdoctoral Science Foundation (Grant No. 2019M661474). JM thanks a Shanghai talent program. QH and HZ thank the support from NSF-DMR- 2003117. The ND experiment was performed at CORELLI of SNS. VR thanks the project funded by Natural Science Foundation of China (Grant No. QN20200009030). A portion of this research used resources at the Spallation Neutron Source, a DOE Office of Science User Facility operated by the Oak Ridge National Laboratory.

SUPPLEMENTARY MATERIAL

The Supplementary Material for this article can be found online at: https://www.frontiersin.org/articles/10.3389/fphy.2021.785801/full#supplementary-material

REFERENCES

1. Tritt TM. Holey and Unholey Semiconductors. *Science* (1999) 283:804–5. doi:10.1126/science.283.5403.804
2. Pei Y, Shi X, LaLonde A, Wang H, Chen L, Snyder GJ. Convergence of Electronic Bands for High Performance Bulk Thermoelectrics. *Nature* (2011) 473:66–9. doi:10.1038/nature09996
3. Kim K, Kim G, Lee H, Lee KH, Lee W. Band Engineering and Tuning Thermoelectric Transport Properties of P-type Bi0.52Sb1.48Te3 by Pb Doping for Low-Temperature Power Generation. *Scripta Materialia* (2018) 145:41–4. doi:10.1016/j.scriptamat.2017.10.009
4. Fu C, Yao M, Chen X, Maulana LZ, Li X, Yang J, et al. Revealing the Intrinsic Electronic Structure of 3D Half-Heusler Thermoelectric Materials by Angle-Resolved Photoemission Spectroscopy. *Adv Sci* (2020) 7:1902409. doi:10.1002/advs.201902409
5. Liu Y, Xie H, Fu C, Snyder GJ, Zhao X, Zhu T. Demonstration of a Phonon-Glass Electron-crystal Strategy in (Hf,Zr)NiSn Half-Heusler Thermoelectric Materials by Alloying. *J Mater Chem A* (2015) 3:22716–22. doi:10.1039/c5ta04418a
6. Shen J, Fu C, Liu Y, Zhao X, Zhu T. Enhancing Thermoelectric Performance of FeNbSb Half-Heusler Compound by Hf-Ti Dual-Doping. *Energ Storage Mater* (2018) 10:69–74. doi:10.1016/j.ensm.2017.07.014
7. Yang Y-X, Wu Y-H, Zhang Q, Cao G-S, Zhu T-J, Zhao X-B. Enhanced Thermoelectric Performance of Bi_2Se_3/TiO_2 Composite. *Rare Met* (2020) 39:887–94. doi:10.1007/s12598-020-01414-4
8. Chen X-K, Pang M, Chen T, Du D, Chen K-Q. Thermal Rectification in Asymmetric Graphene/Hexagonal Boron Nitride van der Waals Heterostructures. *ACS Appl Mater Inter* (2020) 12:15517–26. doi:10.1021/acsami.9b22498
9. Zeng Y-J, Feng Y-X, Tang L-M, Chen K-Q. Effect of Out-Of-Plane Strain on the Phonon Structures and Anharmonicity of Twisted Multilayer Graphene. *Appl Phys Lett* (2021) 118:183103. doi:10.1063/5.0047539
10. Chattopadhyay D, Queisser HJ. Electron Scattering by Ionized Impurities in Semiconductors. *Rev Mod Phys* (1981) 53:745–68. doi:10.1103/RevModPhys.53.745
11. Vandersande JW, Wood C. The thermal Conductivity of Insulators and Semiconductors. *Contemp Phys* (1986) 27:117–44. doi:10.1080/00107518608211003
12. Chen X-K, Chen K-Q. Thermal Transport of Carbon Nanomaterials. *J Phys Condens Matter* (2020) 32:153002. doi:10.1088/1361-648X/ab5e57
13. Perumal S, Roychowdhury S, Biswas K. High Performance Thermoelectric Materials and Devices Based on GeTe. *J Mater Chem C* (2016) 4:7520–36. doi:10.1039/c6tc02501c
14. Xiao Y, Zhao L-D. Charge and Phonon Transport in PbTe-Based Thermoelectric Materials. *Npj Quant Mater* (2018) 3:55. doi:10.1038/s41535-018-0127-y
15. Murugasami R, Vivekanandhan P, Kumaran S, Suresh Kumar R, John Tharakan T. Simultaneous Enhancement in Thermoelectric Performance and Mechanical Stability of P-type SiGe alloy Doped with Boron Prepared by Mechanical Alloying and Spark Plasma Sintering. *J Alloys Compd* (2019) 773:752–61. doi:10.1016/j.jallcom.2018.09.029
16. Masset AC, Michel C, Maignan A, Hervieu M, Toulemonde O, Studer F, et al. Misfit-layered Cobaltite with an Anisotropic Giant Magnetoresistance: $Ca_3Co_4O_9$. *Phys Rev B* (2000) 62:166–75. doi:10.1103/PhysRevB.62.166
17. Yang G, Ramasse Q, Klie RF. Direct Measurement of Charge Transfer in thermoelectricCa3Co4O9. *Phys Rev B* (2008) 78:153109. doi:10.1103/PhysRevB.78.153109
18. Fan M, Zhang Y, Hu Q, Zhang Y, Li X-J, Song H. Enhanced Thermoelectric Properties of Bi2Sr2Co2Oy by Alkali Metal Element Doping and SiC Dispersion. *Ceramics Int* (2019) 45:17723–8. doi:10.1016/j.ceramint.2019.05.341
19. Sakabayashi H, Okazaki R. Crossover from Itinerant to Localized States in the Thermoelectric Oxide $[Ca_2CoO_3]_{(0.62)}[CoO_2]$. *Phys Rev B* (2021) 103:125119. doi:10.1103/PhysRevB.103.125119
20. Naruse K, Kawamata T, Ohno M, Matsuoka Y, Hase M, Kuroe H, et al. Magnetic State of the Geometrically Frustrated Quasi-One-Dimensional Spin System Cu3Mo2O9 Studied by Thermal Conductivity. *J Phys Soc Jpn* (2015) 84:124601. doi:10.7566/jpsj.84.124601
21. Wu Z. Thermal Conductivity Anomaly in Spin-Crossover Ferropericlase under Lower Mantle Conditions and Implications for Heat Flow across the Core-Mantle Boundary. *Am Mineral* (2018) 103:1953–8. doi:10.2138/am-2018-6690
22. Terasaki I, Sasago Y, Uchinokura K. Large Thermoelectric Power in $NaCo_2O_4$ Single Crystals. *Phys Rev B* (1997) 56:R12685–R12687. doi:10.1103/PhysRevB.56.R12685
23. Kurosaki K, Muta H, Uno M, Yamanaka S. Thermoelectric Properties of NaCo2O4. *J Alloys Compd* (2001) 315:234–6. doi:10.1016/s0925-8388(00)01277-9
24. Fujita K., Mochida T., Nakamura K.. High-Temperature Thermoelectric Properties of Na_xCoO_2-Delta Single Crystals. (2001) 40:4644–47. doi:10.1143/jjap.40.4644
25. Jakubczyk EM, Mapp A, Chung CC, Sansom CL, Jones JL, Dorey RA. Enhancing Thermoelectric Properties of NaCo2O4 Ceramics through Na Pre-treatment Induced Nano-Decoration. *J Alloys Compd* (2019) 788:91–101. doi:10.1016/j.jallcom.2019.02.199
26. Zhang L, Liu Y, Tan TT, Liu Y, Zheng J, Yang Y, et al. Thermoelectric Performance Enhancement by Manipulation of Sr/Ti Doping in Two Sublayers of Ca3Co4O9. *J Adv Ceram* (2020) 9:769–81. doi:10.1007/s40145-020-0413-6
27. Iwasaki K, Yamamoto T, Yamane H, Takeda T, Arai S, Miyazaki H, et al. Thermoelectric Properties of Ba3Co2O6(CO3)0.7 Containing One-

Dimensional CoO6 Octahedral Columns. *J Appl Phys* (2009) 106:034905. doi:10.1063/1.3174428
28. Boulahya K, Amador U, Parras M, González-Calbet JM. The Oxycarbonate Ba3Co2O6(CO3)0.60 with a 2H−ABO3-Related Structure. *Chem Mater* (2000) 12:966–72. doi:10.1021/cm991122x
29. Ye F, Liu Y, Whitfield R, Osborn R, Rosenkranz S. Implementation of Cross Correlation for Energy Discrimination on the Time-Of-Flight Spectrometer CORELLI. *J Appl Cryst* (2018) 51:315–22. doi:10.1107/S160057671800403X
30. Morgan Z, Zhou HD, Chakoumakosa B, Ye F. RMC-DISCORD. Reverse Monte Carlo Refinement of DIffuse Scattering and CORrelated Disorder from Single Crystals. *J Appl Crystallogr* (2021) 77:A77–A87. doi:10.1107/s0108767321099128
31. Igarashi H, Shimizu Y, Kobayashi Y, Itoh M. Spin Disorder in an Ising Honeycomb Chain Cobaltate. *Phys Rev B* (2014) 89:054431. doi:10.1103/PhysRevB.89.054431
32. Ando Y, Miyamoto N, Segawa K, Kawata T, Terasaki I. Specific-heat Evidence for strong Electron Correlations in the Thermoelectric material(Na,Ca)Co2O4. *Phys Rev B* (1999) 60:10580–3. doi:10.1103/PhysRevB.60.10580
33. Lu Z, Ge L, Wang G, Russina M, Günther G, dela Cruz CR, et al. Lattice Distortion Effects on the Frustrated Spin-1 Triangular-Antiferromagnet $A_3NiNb_2O_9$ (A=Ba, Sr, and Ca). *Phys Rev B* (2018) 98:094412. doi:10.1103/PhysRevB.98.094412
34. Igarashi K, Shimizu Y, Satomi E, Kobayashi Y, Takami T, Itoh M. Absence of Magnetic Order in Ising Honeycomb-Lattice $Ba_3Co_2O_6(CO_3)_{0.7}$. *J Phys Conf Ser* (2012) 400:032024. doi:10.1088/1742-6596/400/3/032024
35. Koshibae W, Tsutsui K, Maekawa S. Thermopower in Cobalt Oxides. *Phys Rev B* (2000) 62:6869–72. doi:10.1103/PhysRevB.62.6869
36. Che HL, Shi J, Wu JC, Rao X, Liu XG, Zhao X, et al. Thermal Conductivity of Ca3Co2O6 Single Crystals. *AIP Adv* (2018) 8:055811. doi:10.1063/1.5005992
37. Song JD, Wang XM, Zhao ZY, Wu JC, Zhao JY, Liu XG, et al. Low-temperature Heat Transport of $CuFe_{1-x}Ga_xO_2$ (x=0-0.12) Single Crystals. *Phys Rev B* (2017) 95:224419. doi:10.1103/PhysRevB.95.224419
38. Cheng J-G, Zhou J-S, Goodenough JB. Thermal Conductivity, Electron Transport, and Magnetic Properties of Single-crystalCa3Co2O6. *Phys Rev B* (2009) 79:184414. doi:10.1103/PhysRevB.79.184414

Conflict of Interest: The authors declare that the research was conducted in the absence of any commercial or financial relationships that could be construed as a potential conflict of interest.

Publisher's Note: All claims expressed in this article are solely those of the authors and do not necessarily represent those of their affiliated organizations, or those of the publisher, the editors and the reviewers. Any product that may be evaluated in this article, or claim that may be made by its manufacturer, is not guaranteed or endorsed by the publisher.